Quaternary Science Reviews 111 (2015) 51–61

Contents lists available at ScienceDirect

Quaternary Science Reviews

journal homepage: www.elsevier.com/locate/quascirev

Biogeochemical evidence of Holocene East Asian summer and winter monsoon variability from a tropical maar lake in southern China

Guodong Jia [a, b, *], Yang Bai [a, f], Xiaoqiang Yang [c], Luhua Xie [a], Gangjian Wei [a], Tingping Ouyang [a], Guoqiang Chu [d], Zhonghui Liu [e], Ping'an Peng [b]

[a] Key Laboratory of Marginal Sea Geology, Guangzhou Institute of Geochemistry, Chinese Academy of Sciences, Guangzhou, China
[b] State Key Laboratory of Organic Geochemistry, Guangzhou Institute of Geochemistry, Chinese Academy of Sciences, Guangzhou, China
[c] Department of Earth Sciences, Sun Yat-Sen University, Guangzhou, China
[d] Institute of Geology and Geophysics, Chinese Academy of Sciences, Beijing, China
[e] Department of Earth Sciences, The University of Hong Kong, Hong Kong, China
[f] University of Chinese Academy of Sciences, Beijing, China

ARTICLE INFO

Article history:
Received 13 January 2014
Received in revised form
3 January 2015
Accepted 6 January 2015
Available online 22 January 2015

Keywords:
East Asian monsoon
Holocene
Tropical lake record
Isotope proxy
ENSO

ABSTRACT

Lake Huguangyan (21°9′ N, 110°17′ E), a maar lake located near the South China Sea, can provide valuable sedimentary data regarding past changes of the East Asian monsoonal system. Here, we used the proxies of TOC, $\delta^{13}C_{org}$, $\delta^{15}N$, and leaf wax *n*-alkane $\delta^{13}C$ values ($\delta^{13}C_{wax}$) to reconstruct the lake conditions, which, in turn, revealed patterns in monsoonal changes during the Holocene. Two distinct patterns of proxy changes were identified in the sedimentary profile. A marked shift in the $\delta^{13}C_{wax}$ value at ~9.2 ka (thousand years ago) suggests the abrupt disappearance of C_4 plants, signaling the enhancement of East Asian summer monsoon (EASM). Between 9.2 and 1.8 ka, a nearly pure C_3 terrestrial ecosystem was present, with the climax at ca 7–6 ka. After ca 3 ka, fewer tropical species and a reappearance of C_4 plants at 1.8 ka indicate a weakened EASM in the late Holocene. The TOC concentration and $\delta^{15}N$ value proxies appear to be associated with lake aquatic production and upwelled nutrient supply and utilization, which are modulated by, and thus indicative of, the strength of the East Asian winter monsoon (EAWM). The two EAWM records suggest a weakening trend from the early to late Holocene, with the most significant transition at ~6 ka; thus, the EAWM trend was broadly in-phase with that of the EASM. However, the marked EASM intensification at 9.2 ka occurred within the period of a strong EAWM between 10.5 and 6 ka and lagged the monsoonal enhancement as inferred from the Dongge Cave $\delta^{18}O$ values. Our EASM records displays an overall arid-wet-arid pattern, which is in-phase with the hydrological variability in tropical Australia and anti-phase with that in the outer-tropical Andes. These phase relationships might be linked to changes in the thermal state of the tropical Pacific during the Holocene.
© 2015 Elsevier Ltd. All rights reserved.

1. Introduction

Variations in the East Asian monsoon during the Holocene have been extensively studied during the past several decades based on proxy data obtained from various sedimentary records. These studies have been prompted in part by the large population affected by the East Asian monsoon and the alarming rate of the current global climate change. During recent years, there have been several attempts to reconstruct the Holocene history of the East Asian monsoon by compiling and synthesizing published proxy records that are widely distributed in China. These records, however, have displayed inconsistent trends and thus have produced contradictory histories. For example, An et al. (2000) proposed a time-regression hypothesis in which the East Asian summer monsoon (EASM) maximum displayed a trend of southeastward retreat as the extent of summer insolation declined throughout the Holocene. However, this time-regression hypothesis is not supported by numerous subsequent high-resolution studies, as reviewed by Zhao et al. (2009) and Zhang et al. (2011), who suggested a broadly synchronous climatic history across the monsoon region. Nevertheless, an updated perspective of EASM diachronity presented by Ran and Feng (2013) deemed that the strength of the EASM had

* Corresponding author. Guangzhou Institute of Geochemistry, Chinese Academy of Sciences, 511 Kehua Street, Guangzhou 510640, China. Tel.: +86 20 85290157.
E-mail address: jiagd@gig.ac.cn (G. Jia).

http://dx.doi.org/10.1016/j.quascirev.2015.01.002
0277-3791/© 2015 Elsevier Ltd. All rights reserved.

gradually shifted northward during the early Holocene and southward during the late Holocene. The phase relationship between the EASM and the Indian summer monsoon (ISM) is another focus of debate, with distinct viewpoints indicating a generally in-phase (Herzschuh, 2006) relationship and an anti-phase (Wang et al., 2010) relationship between the two monsoonal systems. The reasons for these different opinions are complex, but one reason may be partly associated with the lack of relatively high-resolution tropical monsoon records extending back to at least the early Holocene in southernmost China, which is closest to the moisture source, i.e., the South China Sea (SCS) and adjacent western tropical Pacific.

The East Asian winter monsoon (EAWM), the winter counterpart of the EASM, is the atmospheric flow over East Asia that originates in the Siberian High centered in Mongolia and northeastern Siberia. Past changes in the EAWM have been inferred mainly from grain size records spanning orbital and millennial time scales from the Chinese Loess Plateau (e.g., An et al., 1991; Liu and Ding, 1998; Porter and Zhou, 2006). Many such records from the Holocene indicate a strengthening of the EAWM over time from one of low intensity during the warm early Holocene to one of high intensity during the cool late Holocene (Yang and Ding, 2008). This trend is also suggested by records of Ti concentration, total organic carbon (TOC) concentration and magnetic susceptibility from Lake Huguangyan (HGY), a tropical lake in southern China (Yancheva et al., 2007). However, an opposite trend in the EAWM during the Holocene, i.e., a weakening EAWM from the early to late Holocene, has been recently proposed based on records of diatom assemblages in the same lake (Wang et al., 2012). Reconstructions of the EAWM based on spatial gradients in sea surface temperatures (SSTs) in the SCS (Steinke et al., 2010, 2011; Huang et al., 2011) also support a stronger EAWM during the early Holocene.

Thus, it appears that high-resolution records from tropical East Asia may provide key evidence regarding the evolution of both the EASM and EAWM. Lake HGY is an ideal location for obtaining such records and has become a favored area for such studies by many paleoclimatologists. Until now, only a few sets of sediment cores have been collected for such studies. The first set was collected in 1997 by a team from GeoForschungsZentrum Potsdam and the Chinese Academy of Sciences (Mingram et al., 2004) and was the basis for developing numerous conclusions regarding climate change since the last deglaciation (e.g., Liu et al., 2000; Mingram et al., 2004; Wang et al., 2007; Yancheva et al., 2007; L Wang et al., 2008, 2012). However, as noted by Wu et al. (2012), those studies are all based on a poorly constrained age model of the Holocene sediments that lacks good ^{14}C age control for the period between 8400 and 3800 yrs before present (BP), which is a critical transition period in Holocene climate evolution. By providing a continuous, well-constrained, high-resolution ^{14}C age record from a second set of cores, Wu et al. (2012) pinpointed a marked transition in the TOC level, Rb/Sr ratio and magnetic susceptibility at 6080 yrs BP; the previous age model would have assigned this transition a date of 7800 yrs BP. In addition to these age discrepancies, there are also opposing opinions regarding whether certain environmental proxies in the lake sediment are robust indicators of the EASM or EAWM. The reliability of Ti concentration, TOC level, and magnetic susceptibility as indicators of the EAWM (Yancheva et al., 2007) has been questioned (Zhou et al., 2007, 2009; Wu et al., 2012; Shen et al., 2013), and these trends have instead been interpreted as reflecting the EASM (Wu et al., 2012). This inconsistency in proxy interpretations thus prevents a clear understanding of the phase relationship between the EASM and EAWM.

In this study, records from a new set of cores with well-constrained ^{14}C age determinations from Lake HGY were analyzed. Novel proxies were studied, including stable carbon and/or nitrogen isotope values in bulk samples and higher plant leaf wax *n*-alkanes. Using these proxies, we attempted to develop a better understanding of the evolution of both the EASM and EAWM during the Holocene from a single set of sediment cores. On this basis, a mechanism of variations in the EASM mediated by the El Niño-Southern Oscillation (ENSO) is proposed.

2. Geographical setting, sediment cores, and chronology

Lake HGY (21°9′ N, 110°17′ E, Fig. 1) is a volcanic crater lake (i.e., maar) located near the southernmost tip of mainland China and only 4 km from the present coastline of the SCS (Fig. 1). At present, the lake has a surface area of 2.25 km^2 and a catchment area of 3.2 km^2, with a maximum water depth of ~20 m in the south-central region. The lake is bilobate with a submerged north-south ridge in the south-central area.

The site is directly affected by the monsoon climate, which exhibits seasonal changes in atmospheric circulation and precipitation. During the summer months, i.e., from April to October, the EASM brings a large quantity of rain to this area, accounting for 90% of the mean annual precipitation of ca 1600 mm. In addition, high temperatures and weak winds promote thermal stratification in the lake water column, resulting in low nutrients and phytoplankton levels (Zhang et al., 2008; Wang et al., 2012). During the winter months, i.e., from November to March, a strong cold and dry EAWM from the north and northeast prevails and breaks up the thermal stratification of the lake, causing nutrient-rich bottom water to mix with surface water and thereby leading to an increased abundance of phytoplankton (Zhang et al., 2008; Wang et al., 2012).

In 2009, three vertical cores, designated HGY-2, HGY-6 and HGY-7 and located several meters apart, were collected from the lake bottom below water depths of ~10 m using a modified Livingstone piston corer (Yang et al., 2012). Cores HGY-2 and HGY-6 measured 1.67 and 1.89 m in length, respectively. A few tens of centimeters of the upper sediments of the two cores were lost due to their high water content. Core HGY-7 was obtained beginning at a depth of ~1.5 m below the lake bottom and was 3.68 m long. These three cores were split, and one half from each core was continuously sampled at 1-cm intervals in the laboratory for magnetic susceptibility analysis. The magnetic susceptibility features were clear and

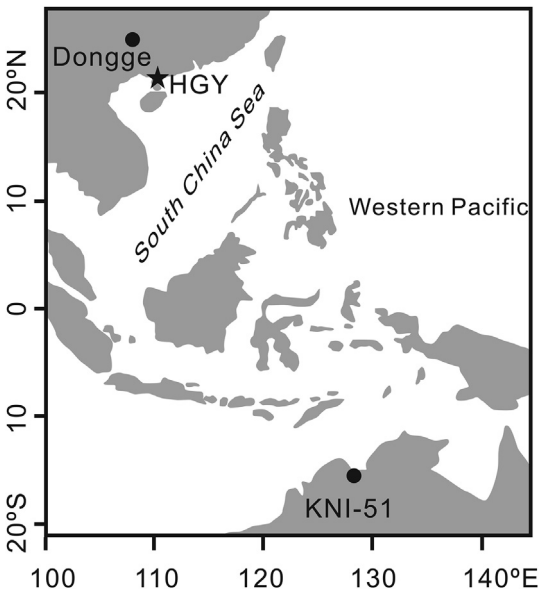

Fig. 1. Location of Lake Huguangyan.

consistent in both cores HGY-2 and HGY-6, and their lower sections overlapped with the upper part of core HGY-7, which allowed for detailed correlation and splicing between the core records (Yang et al., 2012). In this study, a composite of cores HGY-2 and HGY-7 was used. A downcore record of magnetic susceptibility, as presented by Yang et al. (2012), correlates well with previous results by Mingram et al. (2004) and Yancheva et al. (2007).

Radiocarbon age dates of nine mixtures of the lacustrine and terrestrial plant debris from cores HGY-2 and HGY-7 have been published (Yang et al., 2012, Table 1). These samples were processed at the Guangzhou Institute of Geochemistry, Chinese Academy of Science, and analyzed for ^{14}C using accelerator mass spectrometry (AMS) at the Key Laboratory of Heavy Ion Physics, Beijing University. Based on these results, an anomalous age determination of 8890 ± 90 yrs BP for sample 7-117B was ruled out. In this study, five additional bulk samples, including the sample with the anomalous age in the previous analysis, were sent to the Bata Analytic Inc. for AMS ^{14}C analysis. As shown in Fig. 2, data from this second ^{14}C analysis showed a good fit with the depth–age profile from the previous analysis, and the age of 6976 ± 40 yrs BP for sample 7-117B is reasonable. The reason for the anomalous age in the previous analysis is not known, although we accept the reanalysis result for this sample. The agreement between the ^{14}C ages of the plant debris and bulk samples from Lake HGY, which suggests a negligible reservoir age in this freshwater lake, was also confirmed by Wu et al. (2012), who performed several paired analyses of downcore bulk sediments and higher plant macrofossil samples. The age of each downcore sample was calculated using the newly established age model, and the age data mentioned herein are the calibrated values. Based on our ^{14}C age chronology, the onset of the abrupt rise in magnetic susceptibility occurred at ~6.1 ka, which is 1.7 kyrs younger than that obtained by Mingram et al. (2004) but is in agreement with recent results obtained by Wu et al. (2012), who applied a higher-resolution ^{14}C dating method to a core from Lake HGY.

3. Sample analysis

3.1. Bulk parameters

Seventy-seven samples were used for the bulk analysis, which yielded an average temporal resolution of 140 yrs. After the removal of inorganic C using diluted HCl, the samples were analyzed in duplicate for total organic carbon (TOC), total nitrogen (TN), and stable isotopic values ($\delta^{13}C_{org}$ and $\delta^{15}N$) using a Vario Pyro Cube elemental analyzer connected to an Isoprime 100 continuous-flow isotope ratio mass spectrometer (IRMS). The average standard deviations of these measurements were ±0.2% for TOC and TN and ±0.2‰ for $\delta^{13}C_{org}$ and $\delta^{15}N$. The values of $\delta^{13}C_{org}$ and $\delta^{15}N$ are expressed in standard delta notation relative to the Pee Dee Belemnite (PDB) and atmospheric N_2 standards, respectively.

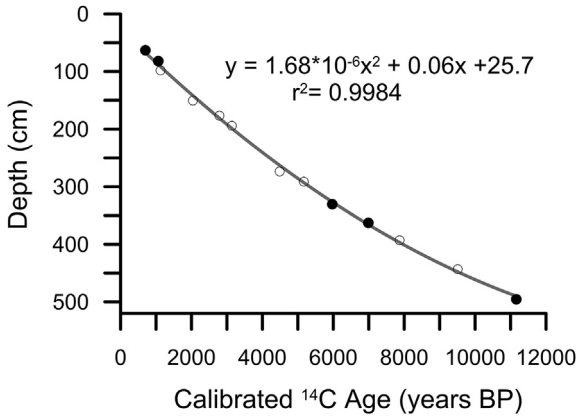

Fig. 2. Depth-age profile of the composite of cores HGY-2 and HGY-7. Circles indicate data from Yang et al. (2012), and filled circles are data from this study.

To further develop an understanding of the source of the organic matter (OM), the residues after organic solvent extraction (see below) were sequentially treated using HCl, HF, and then HCl to remove carbonate and silicate minerals, after which the C and H contents in the dry solids were analyzed using an elemental analyzer. The atomic H/C ratios are reported here.

3.2. $\delta^{13}C$ of long chain n-alkanes

Freeze-dried sediment samples at 2-cm intervals were ultrasonically extracted a total of six times with MeOH (2×), dichloromethane (DCM)/MeOH (1:1, v/v) (2×) and DCM (2×), and all of the extracts were combined after centrifugation. The hydrocarbon fraction was isolated from the total extract using silica gel column chromatography by elution with hexane and then purified for *n*-alkanes using urea adduction. The purified *n*-alkanes were then identified by comparing the retention times determined via gas chromatography (GC) analysis of mixed *n*-alkane standards.

The $\delta^{13}C$ values of the *n*-alkanes were determined by GC-IRMS using an HP 6890 GC system connected to a Delta Plus XL mass spectrometer via a GC-C III interface. Prior to the $\delta^{13}C$ analyses, the CO_2 reference gas was calibrated relative to the PDB. The

Table 1
Radiocarbon dates for the sediment core. All ages were calibrated using the software CalPal (www.calpal.de) with calibration curve INTCAL98.

Sample	Materials	Composite depth (cm)	Conventional ^{14}C age (yrs BP)	Calibrated age (cal. yrs BP)[a]	Laboratory code
2-1A	Bulk organic	62	750 ± 30	696 ± 18	Beta-356769
2-13A	Bulk organic	83	1150 ± 30	1067 ± 56	Beta-356770
2-25B	Plant debris	98	1187 ± 29	1130 ± 40	GZ3750
7-11A	Plant debris	151	2061 ± 28	2040 ± 50	GZ3752
7-25A	Plant debris	177	2666 ± 35	2790 ± 30	GZ3753
2-76B	Plant debris	194	2957 ± 30	3140 ± 60	GZ3751
7-73A	Plant debris	273	4031 ± 28	4490 ± 40	GZ3754
7-82B	Plant debris	291	4484 ± 30	5170 ± 90	GZ3755
7-101A	Bulk organic	330	5200 ± 30	5959 ± 27	Beta-347188
7-117B	Plant debris	362	8010 ± 40	8890 ± 90[b]	GZ3756
7-117B	Bulk organic	362	6100 ± 30	6976 ± 41[b]	Beta-347189
7-132B	Plant debris	393	7010 ± 31	7870 ± 50	GZ3757
7-157A	Plant debris	443	8490 ± 34	9510 ± 30	GZ3758
7-183A	Bulk organic	495	9720 ± 40	11,168 ± 35	Beta-347191

[a] In the text "ka" is used for "cal. kyrs BP".
[b] Data 8890 ± 90 cal. yr BP for sample 7-117B from plant debris is abnormal and replaced by 6976 ± 41 cal. yr BP from reanalysis on bulk organic matter of the sample.

instrument performance was routinely checked using an *n*-alkane standard mixture with known $\delta^{13}C$ values provided by Indiana University. For isotopic standardization, the CO_2 reference gas was automatically introduced into the mass spectrometer in a series of pulses at the beginning and end of each analysis. Each sample was analyzed at least twice, and the average values, with $\sigma < 0.5‰$, are reported here.

4. Results

The *n*-alkane carbon numbers primarily ranged from 19 to 33, with nC_{27}, nC_{29}, and nC_{31} being the most abundant alkanes. A predominance of odd-carbon-numbered compounds was indicated by the carbon preference index ($CPI_{27\text{-}33}$), which varied between 1.6 and 6.8 with a mean value of 4.1. The $\delta^{13}C$ values of the nC_{29} and nC_{31} alkanes ($\delta^{13}C_{29}$ and $\delta^{13}C_{31}$, respectively) displayed long-term stable values between −31.5 ± 0.9‰ and −33.6 ± 0.5‰ between 9.2 and 1.8 ka (Fig. 3b). In contrast, during the two periods of 11.2–9.2 ka and 1.7–0.3 ka, the $\delta^{13}C$ values increased to as high as −25.0‰ for nC_{29} and −21.8‰ for nC_{31}. Interestingly, the $\delta^{13}C_{29}$ values exceeded the $\delta^{13}C_{31}$ values between 9.2 and 1.8 ka but were similar or decreased below the $\delta^{13}C_{31}$ values before and after this lengthy period of time. This pattern can be clearly observed in the temporal changes in the difference between their $\delta^{13}C$ values, designated $\Delta\delta_{31-29}$ (i.e., $\delta^{13}C_{31}-\delta^{13}C_{29}$), as shown in Fig. 3c.

The TOC concentrations were high (5.5–10.5%) with a fluctuating and increasing trend from 11.2 to 6.2 ka. After a marked decrease at 6.2 ka, the TOC level gradually declined to its lowest value of 1.5% in the latest Holocene (Fig. 4a). The TN concentrations ranged from 0.16% to 1.34% and were linearly correlated with the TOC ($TN = 0.11 \times TOC + 0.01$; $R^2 = 0.93$). The TOC/TN ratios varied between 7.0 and 12.5 (Fig. 4b), and the $\delta^{13}C_{org}$ values fluctuated between −25.3‰ and −18.2‰ (Figs. 3a and 4d). Interestingly, the $\delta^{13}C_{org}$ varied with high amplitudes following the pattern of $\delta^{13}C_{29}$ and $\delta^{13}C_{31}$ before 8.0 ka and after 3.2 ka, respectively, but showed elevated values between 8.0 ka and 3.2 ka, during which $\delta^{13}C_{29}$ and $\delta^{13}C_{31}$ remained at low values. The atomic H/C ratios of the insoluble OM were generally >1.2 with markedly higher values during the period of 9.8–6.2 ka (Fig. 4c), similar to the variations in TOC concentrations. Except for a spike of 6.6‰ at 1.3 ka, the $\delta^{15}N$ values varied between 0.4 and 4.7‰ (Fig. 4d). The lowest value of 0.4‰ occurred at 7.8 ka, and values of <3‰ were measured in a section of

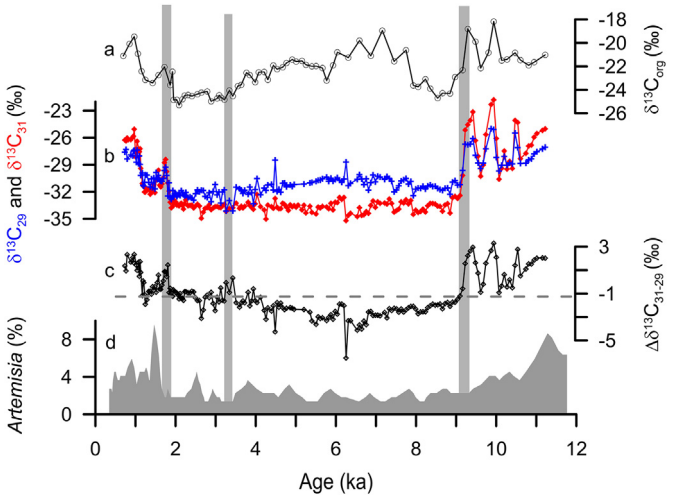

Fig. 3. Time series of leaf wax isotopes and their comparison with other proxies. (a) $\delta^{13}C_{org}$, (b) $\delta^{13}C$ of C_{29} and C_{31} *n*-alkanes, (c) the isotopic difference between C_{31} and C_{29} *n*-alkanes, (d) *Artemisia* percentage from Wang et al. (2007).

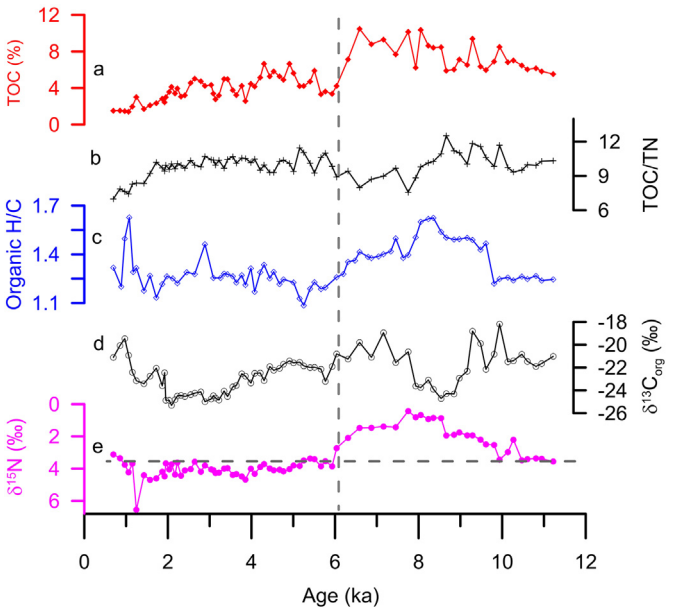

Fig. 4. Time series of bulk parameters. (a) TOC concentration, (b) TOC/TN ratio, (c) atomic H/C ratio of insoluble organic matter, (d) $\delta^{13}C_{org}$ value, and (e) $\delta^{15}N$ value.

core corresponding to the period of time between 10.5 and 6 ka. Before and after this period, nearly all of the $\delta^{15}N$ values were within a narrow range of 3.1–4.7‰.

5. Discussion

5.1. Terrestrial C_3 versus C_4 plants

The predominance of odd-carbon-numbered long chain *n*-alkanes clearly indicates their origins from terrestrial higher plant leaf wax (Eglinton and Hamilton, 1967). The major changes in $\delta^{13}C_{29}$ and $\delta^{13}C_{31}$ record, therefore, could reflect shifts in vegetative photosynthetic pathways, i.e., the relative abundances of C_3 vs. C_4 plants, over time. C_3 plants primarily include trees and shrubs, and C_4 species primarily consist of grasses, and their $\delta^{13}C$ values of leaf wax *n*-alkanes ($\delta^{13}C_{wax}$) range from −28 to −40‰ and from −17 to −25‰, respectively (Collister et al., 1994; Cerling et al., 1997; Chikaraishi and Naraoka, 2003). Therefore, the lengthy period of low $\delta^{13}C_{29}$ and $\delta^{13}C_{31}$ values (<−29‰) between 9.2 and 1.8 ka in our records suggests a steady predominance of C_3 plants in the lake catchment. In contrast, there were periods when C_4 plants were a significant component of the ecosystem both before 9.2 ka and after 1.8 ka (The youngest sample in our records was aged 0.7 ka, not able to reflect current vegetation that is dominated by artificial forest). The expansion of C_4 plants during these two periods can be further confirmed by the positive $\Delta\delta_{31-29}$ values. The underlying reason for this trend is that the nC_{29} alkane is more derived from C_3 plants, whereas the longer-chain nC_{31} counterpart is more contributed by C_4 grasses; therefore, in a mixed C_3/C_4 ecosystem, the $\delta^{13}C_{31}$ value has been found to be less negative than the $\delta^{13}C_{29}$ value (Wang et al., 2013). Conversely, during the period of 9.2–1.8 ka, the $\delta^{13}C_{31}$ values became more negative, suggesting the absence of C_4 plants. Our inferred C_4 plant expansion during the early and late Holocene is broadly consistent with the pollen record of this lake reported by Wang et al. (2007), which exhibits greater abundances of *Artemisia* during those same intervals of the Holocene (Fig. 3d), as many *Artemisia* grasses use the C_4 pathway of carbon fixation.

The relative abundance of C_3 vs. C_4 plants in a regional ecosystem is controlled by the combined effects of the atmospheric CO_2 level (pCO_2), temperature and water availability (Ehleringer, 2005). C_4 photosynthesis involves a carbon-concentrating mechanism, making it more efficient than C_3 photosynthesis in conditions of low pCO_2 levels (Keeley and Rundel, 2003). During the Holocene, however, the pCO_2 level decreased from 268 ppmv at 11 ka to 260 ppmv at 8.2 ka and then monotonically increased during the following 7 kyrs to 285 ppmv (Indermühle et al., 1999). This pattern of pCO_2 changes does not match our *n*-alkane record, which shows a rapid decline in C_4 photosynthesis at 9.2 ka and a C_4 expansion at 1.8 ka, suggesting that pCO_2 was not the dominant factor controlling these shifts in the photosynthetic pathways.

Temperature and water availability also regulate C_3/C_4 plant distributions. C_3 and C_4 plants favor cool and warm temperatures, respectively (Ehleringer, 2005), and in conditions of limited water availability, C_4 plants have a competitive advantage due to their more efficient use of water and higher rates of photosynthesis even upon stomatal closure (Ehleringer et al., 1997; Epstein et al., 1997; Keeley and Rundel, 2003). Reconstructions of the SSTs based on marine sediment cores collected from the northern and coastal SCS show continuously high temperatures (>25 °C) during the Holocene in the adjacent marine environment (Wang et al., 1999; Kong et al., 2014). Based on the tropical conditions at our study site and the proximity to the ocean, we conclude that temperature changes are unlikely to have played a major role in regulating the C_3/C_4 plant distributions. Instead, water availability is the preferred explanation, and the occurrence and expansion of C_4 plants in the early and late Holocene may indicate arid conditions. Similar arguments have also been advanced to explain the causes of C_3/C_4 variations in tropical Africa and Hawaii (Castañeda et al., 2009; Uchikawa et al., 2010). The pollen record from Lake HGY, which displayed a relatively high abundance of *Artemisia* before 9.2 ka and after 1.8 ka (Fig. 3d), also supports the inference of a dry climate during these periods, as *Artemisia* species are usually abundant in arid or semiarid habitats. Alternatively, the post-1.8 ka advancement of C_4 plants might be associated with the increase in human activities, e.g., deforestation and/or the cultivation of C_4 plants, such as sugar cane, during the last 2 kyrs. Similar hypotheses regarding the role of anthropogenic cultivation have also been proposed for the observed rapid increase in bulk sediment $\delta^{13}C$ values at 2 ka in the nearby Pearl River basin (Strong et al., 2013). At present, however, it is difficult for us to resolve the influence of human activity on vegetation. Nevertheless, proxies for the past 2 kyrs in the same lake, such as pollen assemblage, magnetic susceptibility and TOC that are also prone to human disturbance, appear to well reflect the climate changes (Wang et al., 2007; Yancheva et al., 2007; Wu et al., 2012). So, in this study $\delta^{13}C_{wax}$ in the late Holocene is tentatively interpreted to reflect climate change as well.

Moreover, even for the predominant C_3 ecosystem during the period of 9.2–1.8 ka, there might be some vegetation changes as implied by variations in $\Delta\delta_{31-29}$ record. In the record, $\Delta\delta_{31-29}$ decreased from 9.2 ka to 6.5 ka and then turned into increase toward the late Holocene. (Fig. 3c). At present, we are not aware of any vegetational implications of the $\Delta\delta_{31-29}$ values for a C_3 ecosystem. Based on our measurements of the $\delta^{13}C_{wax}$ values from

Table 2
$\delta^{13}C$ values of C_{29} and C_{31} *n*-alkanes (‰, relative to PDB) for C_3 plants in the tropical-subtropical east Asia.

Sampling site	Plant family	Plant genera and species	$\delta^{13}C_{29}$	$\delta^{13}C_{31}$	$\Delta\delta^{13}C_{31-29}$	Reference[a]
Tropical-south subtropical						
15° N, 100° E	Euphorbiaceae	*Manihot utilissima*	−30.8	−32.0	−1.2	3
21.1° N, 110.3° E	Solanaceae	*Solanum nigrum*	−30.0	−30.4	−0.4	1
21.1° N, 110.3° E	Fabaceae	*Mimosa pudica*	−33.5	−34.7	−1.2	1
21.1° N, 110.3° E	Fabaceae	*Bauhinia variegata*	−37.6	−38.2	−0.6	1
21.1° N, 110.3° E	Cupressaceae	*Taxodium distichum*	−31.6	−32.3	−0.7	1
21.1° N, 110.3° E	Theaceae	*Schima kwangtungensis*	−30.4	−31.7	−1.2	1
23.1° N, 113.3° E	Amaranthaceae	*Alternanthera bettzickiana* (Regel) Nichols.	−36.5	−37.2	−0.7	2
23.1° N, 113.3° E		*Alternanthera dentata ' Rubiginosa '*	−36.6	−37.2	−0.6	2
23.1° N, 113.3° E		*Alternanthera versicolor Regel*	−36.7	−37.5	−0.8	2
23.1° N, 113.3° E	Araucariaceae	*Araucaria cunninghamii Sweet*	−30.1	−30.5	−0.4	2
23.1° N, 113.3° E	Lauraceae	*Cinnamomum burmannii* (Nees) Bl.	−33.3	−37.2	−3.9	2
23.1° N, 113.3° E	Euphorbiaceae	*Euphorbia pulcherrima* Willd.	−38.0	−37.4	0.6	2
23.1° N, 113.3° E	Moraceae	*Ficus altissima* Bl.	−33.9	−36.1	−2.2	2
23.1° N, 113.3° E		*Ficus microcarpa* Linn. f.	−31.0	−33.1	−2.1	2
23.1° N, 113.3° E	Verbenaceae	*Holmskioldia sanguinea* Retz.	−35.3	−33.8	1.5	2
23.1° N, 113.3° E	Bignoniaceae	*Kigelia africana* (am.) Benth.	−33.1	−33.3	−0.2	2
23.1° N, 113.3° E	Oleaceae	*Osmanthus fragrans* Lour.	−35.7	−37.0	−1.3	2
23.1° N, 113.3° E	Meliaceae	*Swietenia mahagoni* (L.) Jacq.	−34.1	−35.9	−1.8	2
27°N, 142° E	Fabaceae	*Albizia julibrissin*	−35.9	−37.8	−1.9	3
		Average	−34.0 ± 2.7	−34.9 ± 2.6	−0.9 ± 1.3	
North subtropical						
35.5° N,139.5° E	Theaceae	*Camellia sasanqua*	−31.3	−33.1	−1.8	3
35.5° N,139.5° E	Cupressaceae	*Chamaecyparis obtusa*	−30.6	−30.0	0.6	3
35.5° N,139.5° E	Pinaceae	*Pinus thunbergii*	−33.5	−34.1	−0.6	3
35.5° N,139.5° E	Fagaceae	*Quercus acutissima*	−34.7	−34.8	−0.1	3
36.5° N 138.5° E	Sapindaceae	*Acer argutum*	−35.8	−36.2	0.4	3
36.5° N 138.5° E		*Acer carpinifolium*	−36.4	−36.2	0.2	3
36.5° N 138.5° E		*Acer palmatum*	−40.5	−41.8	−1.3	3
36.5° N 138.5° E	Asteraceae	*Artemisia princeps*	−36.5	−35.2	1.3	3
36.5° N 138.5° E	Asteraceae	*Taraxacum officinale*	−37.0	−36.4	0.6	3
36.5° N 138.5° E	Cornaceae	*Benthamidia japonica*	−37.6	−36.9	0.7	3
36.5° N 138.5° E	Cupressaceae	*Cryptomeria japonica*	−32.3	−30.4	1.9	3
36.5° N 138.5° E	Plantaginaceae	*Plantago asiatica*	−39.6	−39.8	−0.2	3
36.5° N 138.5° E	Rosaceae	*Prunus jamasakura*	−34.2	−33.5	0.7	3
36.5° N 138.5° E		*Quercus dentata*	−33.5	−34.4	−0.9	3
36.5° N 138.5° E		*Quercus mongolica*	−33.4	−32.2	1.2	3
		Average	−35.1 ± 2.9	−35 ± 3.1	0.2 ± 1.0	

[a] 1. This study; 2. Bi et al. (2005); 3. Chikaraishi and Naraoka (2003).

several living C_3 specimens in the Lake HGY catchment and previously published data from tropical to temperate zones of East Asia (Chikaraishi and Naraoka, 2003; Bi et al., 2005) (Table 2), we observed that the $\Delta\delta_{31-29}$ values vary between −3.9‰ and +1.9‰; those values of evergreen plants in the tropical-south subtropical area (−0.9 ± 1.3‰) are more negative on average than those of deciduous plants in the north subtropical-temperate area (+0.2 ± 1.0‰). Based on these limited data, we tentatively suggest that our $\Delta\delta_{31-29}$ record from the period between 9.2 and 1.8 ka likely indicate vegetation dynamics within a C_3 ecosystem. Specifically, the decreasing trend in $\Delta\delta_{31-29}$ values before 6.5 ka may suggest a wetting and warming trend toward the mid Holocene, and conversely, the increasing trend after that time may indicate a drying and cooling trend toward the late Holocene. So, the lowest $\Delta\delta_{31-29}$ values at 7–6 ka may imply a climax of tropical rainforest, suggestive of climatic optimum during the Holocene.

5.2. Lacustrine carbon dynamics

The TOC/TN ratio is frequently used to characterize sedimentary OM and to discern its biological origin, i.e., aquatic phytoplankton vs. terrestrial higher plants. Conventionally, plants of aquatic origin are believed to have a C/N ratio of less than 10–12, whereas those of terrestrial origin are thought to have a C/N ratio exceeding 20 (Meyers, 1997). However, there is no exact value of TOC/TN separating aquatic from terrestrial plants due to factors such as the degree of N limitation for plant growth and selective loss of N during OM sedimentation. For example, Talbot and Lærdal (2000) reported values exceeding 19.6 in material of a phytoplankton origin in severely N-deficient conditions in Lake Victoria, Africa. Nearly all of the TOC/TN ratios in our samples were less than 12, indicating a predominantly aquatic origin of the sedimentary OM. This finding is further supported by the atomic H/C ratios of the insoluble OM that were >1.2 in nearly all of the samples, which is analogous to type II and I kerogen originating from mixed phytoplankton, zooplankton, and bacterial debris (Peters and Moldowan, 1993). Moreover, the markedly higher H/C ratios in OM during the period of 10–6.2 ka coincide with the higher TOC values, suggesting greater algal contributions and/or better OM preservation. Better OM preservation in anoxic lake bottom as a result of a stagnant water column and weak EAWM during the early and middle Holocene has been suggested by Yancheva et al. (2007). However, subsequent studies of diatom assemblages in the same sediment materials revealed a stronger EAWM and water column mixing during this period (L Wang et al., 2008, 2012). Therefore, the higher values of H/C ratio and TOC concentration prior to 6.2 ka may be primarily associated with enhanced algal input, and thus the TOC concentration may be used as an estimate of paleoaquatic productivity in the lake, as suggested by Wu et al. (2012) for this lake.

Given that the downcore organic matter is predominantly of aquatic origin and any terrestrial contribution is insignificant, it is surprising that the $\delta^{13}C_{org}$ record is highly consistent with the $\delta^{13}C_{wax}$ records of the land vascular plants during the period of 11–8 ka and after 3.2 ka (Fig. 3a, b), when remarkable shifts occurred in the $\delta^{13}C$ values of the terrestrial vegetation. This relationship suggests that the $\delta^{13}C_{org}$ record was primarily forced by processes within or external to the lake that may be indirectly associated with regional changes in the terrestrial flora. Because this lake is located in a silicate basin with a productive soil mantle, the dissolved inorganic carbon (DIC) in the lake water is likely recharged by river and groundwater DIC that is primarily derived from CO_2 from the surrounding soils, the isotopic composition of which ultimately depends on the type of vegetation (Telmer and Veizer, 1999; Karim and Veizer, 2000; Wachniew, 2006). In addition, riverine dissolved organic carbon (DOC), which may be rapidly recycled in the lacustrine ecosystem, could also be closely linked to the isotopic composition of the soil OM in the catchment, as has been observed elsewhere (Quay et al., 1992; Brunet et al., 2009). We therefore hypothesize that the lake water DIC, which is the primary C source for the aquatic algal assimilation, was isotopically determined by changes in the catchment vegetation. This hypothesis may be supported by the aforementioned agreement between the ^{14}C ages of the plant debris and bulk OM in the lake sediments, indicating a negligible reservoir age in this freshwater lake. Thus, a regional change in terrestrial vegetation $\delta^{13}C$ would result in a responsive change in the lake water $\delta^{13}C_{DIC}$, and ultimately, in the $\delta^{13}C$ of the photosynthesized organic C by aquatic phytoplankton. A similar hypothesis has also been presented for the decreases of 5–8‰ in lacustrine $\delta^{13}C$ values during the terminal Pleistocene and early Holocene in tropical Lakes Victoria, Albert and Tanganyika in Africa (Talbot et al., 2006).

However, there is a remarkable incongruity between the $\delta^{13}C_{org}$ and $\delta^{13}C_{wax}$ records during the period of ca 8–3 ka, when the $\delta^{13}C_{org}$ values were significantly elevated and no longer followed the pattern of $\delta^{13}C_{wax}$ that remained steadily at low values. This mismatch suggests that $\delta^{13}C_{org}$ were not simply modulated by terrestrial $\delta^{13}C$ alone during this period, and factors other than external vegetation changes are responsible for the $\delta^{13}C_{org}$ variations. Indeed, in addition to the $\delta^{13}C_{DIC}$, internal processes, such as dissolved CO_2 availability, kinetic carbon isotope fractionation during photosynthesis, and phytoplankton assemblages and growth rates, are also important factors affecting $\delta^{13}C_{org}$ values (e.g., Rau et al., 1992; Laws et al., 1995; Burkhardt et al., 1999; Lehmann et al., 2004). Atmospheric CO_2 and lake water pH could affect the level of dissolved CO_2 but are unlikely to be important due to a lack of evidence of significant changes in these parameters during the studied period. Nevertheless, we noted that the elevated $\delta^{13}C_{org}$ values during the period of ca 8–3 ka largely coincide with the relatively high TOC concentrations, with peak values occurring at ca 7 ka and decreasing trends in the middle-late Holocene (Fig. 4a, d). This concurrence suggests that the changes in $\delta^{13}C_{org}$ values during this period are closely associated with the production of OM. Preferential utilization of ^{12}C during photosynthesis at times of intense algal production may result in progressive isotopic enrichment of the residual DIC pool, and in turn, lead to increasing $\delta^{13}C$ values in successive OM produced from the residual DIC pool. So, the elevated $\delta^{13}C_{org}$ and its dissimilarity with the trend of $\delta^{13}C_{wax}$ during the period of ca 8–3 ka may suggest tight supply of DIC or CO_2 relative to aquatic productivity.

5.3. Nitrogen processes

The assimilation and cycling of nitrogen in a lake and its surrounding catchments are complex processes. The history of these processes may be tracked by means of sedimentary $\delta^{15}N$ due to its ability to reflect several processes that can affect the eventual isotopic values. The intercept of the linear relationship between the TOC and TN concentrations at zero TOC is 0.01%, which is much lower than the TN concentration (0.16–1.34%) in the samples from this study and is thus suggestive of a close association between the TN and OM. Because the sedimentary OM is predominantly of aquatic origin, the accumulated N in the lake sediments was likely fixed primarily in the water column via N assimilation. Therefore, the $\delta^{15}N$ values of the fixed N are dependent on the isotope signature of dissolved inorganic nitrogen (DIN) and/or the degree of DIN utilization. In conditions of greater DIN availability, ^{14}N is preferentially utilized by aquatic algae, producing isotopically lighter OM than the DIN reservoir (Wada and Hattori, 1978; Waser et al., 1998; Liu et al., 2013). However, when DIN is a limiting

nutrient and is completely utilized in the upper water column, there would be no isotopic fractionation between the DIN and organic N. In such a case, the $\delta^{15}N$ value in sediments can be used as a proxy for the DIN isotope composition, which may be controlled by several complex processes. Such processes include microbial denitrification with a large fractionation effect producing strongly enriched residual DIN pools (Mariotti et al., 1988) and N_2 fixation involving little or no isotopic fractionation by cyanobacteria (Fogel and Cifuentes, 1993).

A remarkable feature of the $\delta^{15}N$ record from Lake HGY is the persistently low values during the period of 10.5–6 ka, with a minimum at approximately 8 ka (Fig. 4e). Temporal variations in the $\delta^{15}N$ record are largely negatively correlated with the TOC record, with the prominent low $\delta^{15}N$ values coinciding with the high TOC values. The $\delta^{15}N$ record is also negatively correlated with the $\delta^{13}C_{org}$ record associated with OM production during the period of 8–3 ka. Therefore, the variations in $\delta^{15}N$ may be associated with OM production in the lake. Elevated productivity prior to ~6 ka may have been induced by higher DIN levels in the upper water column due to an abundant N supply from external sources, such as the wash-in of soil nutrients and fixation of atmospheric N_2, and/or from upwelled bottom water maintained by strong wind-induced vertical mixing. The TOC content in cores from Lake HGY has been used as an indicator of the EASM (Wu et al., 2012), the underlying explanation being that the heavy precipitation induced by the summer monsoon would increase the supply of nutrients to the lake, resulting in increased aquatic production and thus a high TOC content in the lake sediments. However, this mechanism appears to be implausible because the TOC increase and the $\delta^{15}N$ decrease at ca 10.5 ka precedes the intensification of the moisture increase at 9.2 ka inferred from our $\delta^{13}C_{wax}$ records (Fig. 5). Atmospheric N_2 fixation is another important external N source that has been cited as an explanation for the low sedimentary $\delta^{15}N$ values in lakes of East Africa and elsewhere during the late Pleistocene and early Holocene (Talbot and Lærdal, 2006; McLauchlan et al., 2013). This process of N_2 fixation involves little isotopic fractionation and produces OM with typical $\delta^{15}N$ values of approximately $0 \pm 2‰$ that are similar to the lowest values in our $\delta^{15}N$ record. However, N_2-fixing cyanobacteria are most likely found in conditions of N deficiency and stable lake water stratification, which contradicts the recent findings of strong winter wind stress and the resultant water column mixing and nutrient upwelling conditions between 13 and 5 ka in Lake HGY (Wang et al., 2012). Therefore, an internal DIN supply from upwelled deep water due to water column destratification and mixing by cold and strong winter wind is favored as the primary cause of the high DIN levels that support the high productivity prior to 6.2 ka. The prominent low $\delta^{15}N$ values coinciding with the high productivity may imply that the upwelled DIN pool was so large that aquatic algae were unable to deplete it completely, thus leading to the synthesis and accumulation of ^{15}N-depleted OM.

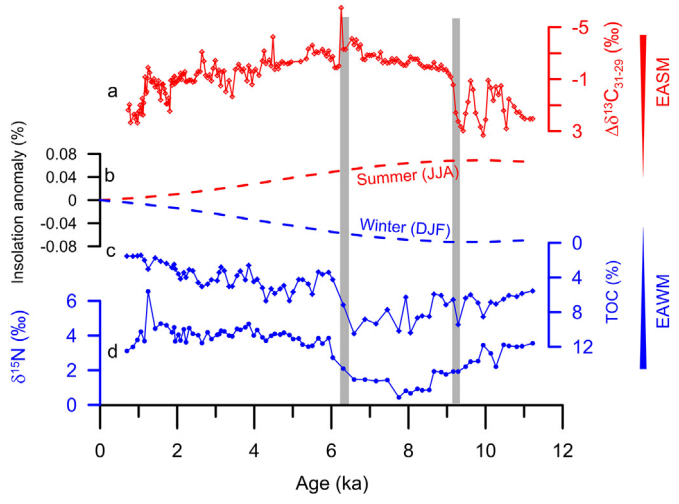

Fig. 5. Changes of monsoon proxies and solar insolation during the Holocene. (a) the isotopic difference between C_{31} and C_{29} *n*-alkanes as proxy of EASM, (b) Summer and winter insolation anomalies at 20° N relative to present level (Berger and Loutre, 1991), (c) TOC concentration and (d) $\delta^{15}N$ value as proxies of EAWM.

5.4. Phase relationship between the EAWM and EASM

The forgoing discussion demonstrates that DIN availability from the upwelled deep water determines aquatic primary production, as indexed by the downcore TOC concentration, and $\delta^{15}N$ values. The nutrient upwelling conditions depend on water column status that is controlled by temperature and wind strength, with water column mixing and intensive upwelling of DIN occurring in cold and strong wind conditions during winter. Therefore, TOC and $\delta^{15}N$ may be used as a measure of the EAWM; and both the TOC and $\delta^{15}N$ records imply a strong EAWM between 10.5 and 6.2 ka followed by a rapid transition to a weak EAWM into the late Holocene (Fig. 5c, d). This changing pattern of the EAWM, although discordant with the findings showing strengthening of the EAWM during the Holocene (e.g., Yancheva et al., 2007; Yang and Ding, 2008), is consistent with evidence from sedimentary diatom assemblages controlled by winter monsoon intensity in the same lake (L Wang et al., 2008, 2012). Stronger EAWM during the early-middle Holocene than during the late Holocene is also indicated by sedimentary records in the nearby SCS (Steinke et al., 2010, 2011; Huang et al., 2011). The reconstructed SSTs in the open SCS using C_{37} alkenone thermometer show almost continuous increases over the Holocene (e.g., Wang et al., 1999; Kong et al., 2014). As alkenone SSTs may be biased toward wintertime SSTs in low latitudes (e.g., Leduc, et al., 2010; Huang et al., 2011), its increasing trend during the Holocene could also suggest a weakening history of EAWM. Further, it is clear that the weakening trend of EAWM during the Holocene is in accordance with the persistent increase of winter insolation at northern Hemisphere (Fig. 5b), suggesting a causal link between them.

A general trend of weakening of EASM from the early-middle Holocene to the late Holocene has long been recognized and is also indicated by our $\Delta\delta_{31-29}$ record indicative of vegetation and moisture changes in the catchments of Lake HGY (Fig. 5a). So there is a broadly in-phase relationship between the EAWM and EASM in millennial time scales, likely reflecting a stronger seasonal contrast during the early-middle Holocene than during the late Holocene. This stronger seasonal contrast during the early-middle Holocene is clearly demonstrated in the comparison of solar insolation between winter and summer seasons (Fig. 5b). Several authors also proposed that a strong seasonal contrast in solar insolation and the presence of residual ice sheets during the early Holocene may have caused the strong EAWM during that time (L Wang et al., 2008; Huang et al., 2011).

Nevertheless, the EASM does not vary synchronously with the EAWM. For example, the marked disappearance of C_4 plants in the lake catchments at ca 9.2 ka, a signal of southerly moisture enhancement, occurred within the lengthy period of higher TOC concentrations and lower $\delta^{15}N$ values between 10.5 and 6.2 ka suggestive of a stronger EAWM. Moreover, the suggested southerly moisture enhancement at ca 9.2 ka evidently lagged the high summer insolation during early Holocene (Fig. 5a, b). These timing disparities may indicate a separate driving mechanism for the EASM during the Holocene, as discussed below.

5.5. Mediation of the EASM by the ENSO

Overall, the $\delta^{13}C_{wax}$ trends, especially the $\Delta\delta_{31-29}$ record, in this study indicate that environmental moisture levels increased at ~9.2 ka, reached the highest level at ~7–6 ka, and then gradually declined toward the late Holocene, displaying an arid-wet-arid climate pattern over the Holocene (Fig. 6e). Compared to the abrupt decrease in oxygen isotope ($\delta^{18}O$) values prior to 10.5 ka in stalagmites from the Dongge Cave (25° N, 108° E; Fig. 1) (Fig. 6d; Dykoski et al., 2005), the early Holocene arid-to-wet transition at approximately 9.2 ka in our records apparently occurred later. Similarly, based on a comprehensive synthesis of pollen records in the area of the East Asian monsoon, Zhao et al. (2009) found that environmental moisture levels remained relatively low during the first two millennia of the Holocene until approximately 9.5 ka, after which they reached a maximum between 9.5 and 6 ka. The formation of palaeosols in aeolian sequences, suggestive of increased moisture availability, in the Hunshandake Sandy Land in northern China began at ca 9.6 ka and ended at ca 3 ka (Yang et al., 2013), also consistent with our $\delta^{13}C_{wax}$-inferred EASM history. A later response to insolation by the EASM than by the Indian summer monsoon (ISM) has been suggested by several authors (e.g., Wang et al., 2010; Ran and Feng, 2013). Based on a statistical meta-analysis of moisture patterns in monsoonal central Asia, Wang et al. (2010) found that the moisture evolution in the ISM area roughly followed a maximum in the Northern Hemisphere summer insolation during the early Holocene, whereas the EASM area in mid-latitude China remained relatively dry in the early Holocene and reached its maximum moisture levels between 7 and 4 ka. It is likely that the earlier enhancement of the ISM with its isotopically lighter character was imprinted on the isotopic variations in speleothems in China (Maher, 2008; Maher and Tompson, 2012).

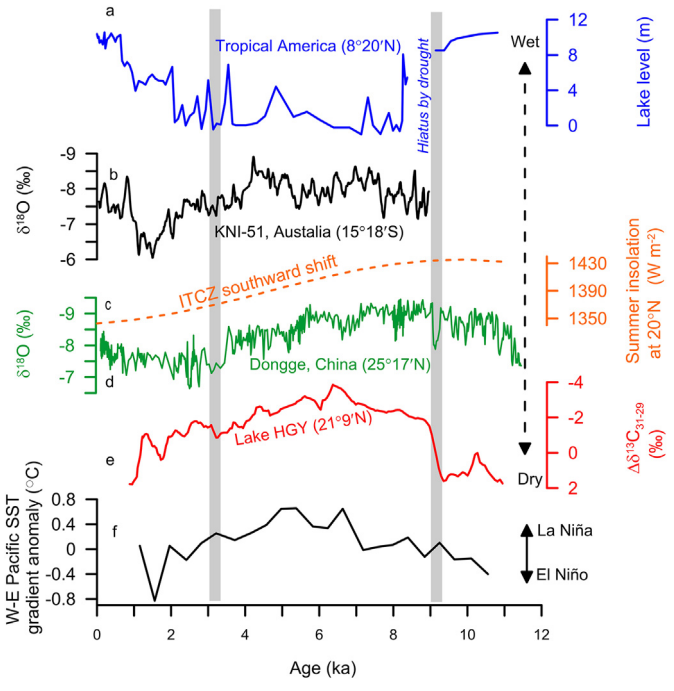

Fig. 6. Holocene hydrologic variability at various sites and comparisons with summer insolation and the thermal state of the tropical Pacific. (a) the lake level of Laguna Blanca in the Venezuelan Andes (Polissar et al., 2013), (b) $\delta^{18}O$ from cave KNI-51 in northwest Australia (Denniston et al., 2013), (c) summer solar insolation at 20°N in the Northern Hemisphere (Berger and Loutre, 1991), (d) $\delta^{18}O$ from Dongge Cave in southern China (Dykoski et al., 2005), (e) the isotopic difference between C_{31} and C_{29} *n*-alkanes in Lake HGY (curves are 7-point running averages), and (f) the zonal sea surface temperature gradient in the equatorial Pacific, indicating ENSO variations, during the Holocene (Koutavas and Joanides, 2012).

Holocene variations in the monsoonal moisture balance on millennial or longer time-scales have been ascribed to orbitally induced changes in solar insolation and subsequent shifts in the position of the Intertropical Convergence Zone (ITCZ) (Fig. 6c) (e.g., Haug et al., 2001; Wang et al., 2005; Koutavas et al., 2006; Fleitmann et al., 2007; Conroy et al., 2008; Chiang and Friedman, 2012). The Dongge Cave $\delta^{18}O$ record, which exhibits evidence of a long-term mid-Holocene weakening of the summer monsoon, has been cited as compelling evidence for the southward shift of the ITCZ (Dykoski et al., 2005; Wang et al., 2005). However, our finding of the arid-wet-arid pattern of EASM during the Holocene calls into question the dominant role of the ITCZ migration in modulating the EASM variability because this arid-wet-arid climate pattern fundamentally differs from that predicted by the southward shift of the ITCZ since the early Holocene. Further evidence contradicting a simple response to the ITCZ position is provided by speleothem $\delta^{18}O$ values (Fig. 6b) in tropical Australia (15° S, 129° E; Fig. 1), which is the counterpart of the tropical East Asia in the southern hemisphere and displays a broadly in-phase relationship with the EASM records (Denniston et al., 2013). This in-phase behavior on either side of the equator could not have been caused by the ITCZ migration because moisture responses to the ITCZ positions are of opposite phase between the northern and southern hemispheres. Likewise, synchronous Holocene climate trends with the same direction in the outer-tropical Andes of the northern and southern hemispheres also challenge the dominant role of a meridional displacement of the ITCZ (Polissar et al., 2013). Furthermore, Holocene climate evolution in the outer-tropical Andes spanning both hemispheres exhibits a wet-arid-wet pattern (Fig. 6a), and the mid-Holocene aridity has also been observed in Hawaii and the Great Basin and Rocky Mountains of the western United States (Benson et al., 2002; Bacon et al., 2006; Shuman et al., 2009; Uchikawa et al., 2010). So, the Holocene climate pattern east of the tropical Pacific is just opposite to what is observed in its west counterpart, including the lake HGY in this study and the tropical Australia reported by Denniston et al. (2013).

The observed in-phase and anti-phase hydrological variability between terrestrial climatic records on either side of the equator and the zonal Pacific, respectively, argue for a consistent driving mechanism during the Holocene. Here, we hypothesize that the thermal state of the tropical Pacific, analogous to the ENSO, mediates the millennial variability of EASM. The EASM precipitation today is greatly influenced by the ENSO state and subtropical high position associated with the SSTs in the western Pacific warm pool (WPWP). During the El Niño phase with colder SSTs in the WPWP, the convective activities may weaken around the SCS and the Philippines, causing the subtropical high to shift southward and, in turn, causing drought in southern and northern China and flooding in central China; the inverse would occur during the La Niña phase (Huang and Wu, 1989; Zhao, 1996; Tao and Zhang, 1998; Gao and Wang, 2012). In addition, landfalls of tropical cyclones, which may bring heavy rainfall accounting for 10–40% of the annual precipitation in southern China (YM Wang et al., 2008), are significantly reduced during El Niño years and increased during La Niña years (Wu et al., 2004). By extending the present-day relationship between the ENSO and EASM precipitation to interpretations of millennial-scale climate variability, although this may be subject to time-scale differences and other climate forcing variations, we surmise that the arid-wet-arid climate pattern in southern and northern China, as suggested by our records and others' (e.g., Yang et al., 2013), is conditioned by the mean state shifts, i.e., El Niño-La Niña-El Niño, of the tropical Pacific. This surmise is also applicable to central China, where the present-day

hydrological conditions are opposite to those in its north and south sides during the ENSO events, and where arid conditions have been found to occur during the period of 7–3 ka and wet conditions thereafter (Xie et al., 2013). Our surmise of the mean state shifts of the tropical Pacific is consistent with numerous paleo ENSO reconstructions spanning the equatorial Pacific (Clement et al., 2000; Moy et al., 2002; McGregor and Gagan, 2004; Koutavas et al., 2006; Koutavas and Joanides, 2012; Carré et al., 2014). For example, a more sustained La Niña mean state, as suggested by a higher W–E Pacific SST gradient, during the middle Holocene has been indicated by Koutavas and Joanides (2012) (Fig. 6f). A reconstruction of ENSO in the eastern tropical Pacific spanning the past 10 kyrs derived from $\delta^{18}O$ values in fossil mollusk shells from Peru also shows that ENSO variance was similar in the early and late Holocene and severely damped ~5 to 4 ka (Carré et al., 2014). Polissar et al. (2013) suggested that ENSO-modulated moisture variability in the outer-tropical Andes of both hemispheres, with higher precipitation during the La Niña phase and vice versa during the El Niño phase, would be pervasive throughout the Holocene. Similarly, the ENSO is also conjectured to have played a dominant role in driving the Holocene Indonesian-Australian summer monsoon variability in the Australian tropics, where wet conditions prevailed during the middle Holocene (Denniston et al., 2013). Both the studies by Polissar et al. (2013) and Denniston et al. (2013), conducted on either side of the tropical Pacific, indicate a mean state of sustained La Niña conditions during the middle Holocene and increases in El Niño strength or frequency during the late Holocene, which is consistent with our surmise presented here.

However, the timing of ca 9.2 ka for the marked intensification of the EASM in our records is not reflected by a corresponding change in the W–E Pacific SST gradient, although the gradient shows an increasing phase during the early Holocene (Fig. 6f). We note that this timing approximately coincides with the beginning of the southward opening of the semi-enclosed SCS at 9.5 ka due to flooding of the Sunda shelf when the rising post-glacial sea level reached −30 m (Linsley et al., 2010). It is likely that the expanded areas of tropical water after this flooding, together with the concurrent SST rise, helped to greatly enhance the convective activity around the SCS and Philippines that favored the intensification of the EASM.

6. Conclusions

Variations in the EASM and EAWM during the Holocene were reconstructed and discussed using multiple proxy records from a well-constrained ^{14}C-dated core from Lake HGY. Leaf wax *n*-alkane $\delta^{13}C$ values are indicators of terrestrial ecosystem photosynthetic pathways, which are ultimately associated with the moisture availability and thus the strength of the summer monsoon. Based on the $\delta^{13}C_{wax}$ records, the EASM was relatively weak during the first half of the early Holocene, intensified rapidly at 9.2 ka to initiate a protracted wet climate until ~3.0 ka, and became weaker again during the late Holocene. The TOC concentration and $\delta^{15}N$ values are suggestive of the levels of aquatic production and the upwelled nutrient supply and utilization, which are associated with cold wind-induced water column disturbance and are thus indicative of the EAWM. The EAWM records are broadly in-phase with the EASM, which display a trend of decreasing strength from the early to late Holocene, with the most significant transition at ~6 ka.

By comparison, the onset of the EASM intensification at 9.2 ka lagged both the strong EAWM and the monsoon enhancement indicated by Dongge Cave $\delta^{18}O$ values, suggesting a distinct driving mechanism for the EASM evolution. Variations in the EASM during the Holocene in the study area displays an overall arid-wet-arid pattern. This pattern is in-phase with the hydrological variability in tropical Australia and anti-phase with that in the outer-tropical Andes, which may be predominantly mediated by mean state shifts in the tropical Pacific zonal thermal gradient.

Acknowledgments

This research was supported by the Strategic Priority Research Program of the Chinese Academy of Sciences (Grant No. XDA05080404), the National Basic Research Program of China (2010CB833405) and “135” project of Guangzhou Institute of Geochemistry (Y234091001). Three anonymous reviewers are thanked for their helpful comments. This is contribution no. IS-2012 from GIGCAS.

References

An, Z.S., Kukla, G., Porter, S.C., Xiao, J.L., 1991. Late Quaternary dust flow on the Chinese Loess Plateau. Catena 18 (2), 125–132.
An, Z.S., Porter, S.C., Kutzbach, J.E., Wu, X.H., Wang, S.M., Liu, X.D., Li, X.Q., Zhou, W.J., 2000. Asynchronous Holocene optimum of the East Asian monsoon. Quat. Sci. Rev. 19, 743–762.
Bacon, S.N., Burke, R.M., Pezzopane, S.K., Jayko, A.S., 2006. Last glacial maximum and Holocene lake levels of Owens Lake, eastern California, USA. Quat. Sci. Rev. 25, 1264–1282.
Benson, L., Kashgarian, M., Rye, R., Lund, S., Paillet, F., Smoot, J., Kester, C., Mensing, S., Meko, D., Lindstrom, S., 2002. Holocene multidecadal and multicentennial droughts affecting Northern California and Nevada. Quat. Sci. Rev. 21, 659–682.
Berger, A., Loutre, M.F., 1991. Insolation values for the climate of the last 10 million years. Quat. Sci. Rev. 10, 297–317.
Bi, X., Sheng, G., Liu, X., Li, C., Fu, J., 2005. Molecular and carbon and hydrogen isotopic composition of n-alkanes in plant leaf waxes. Org. Geochem. 36, 1405–1417.
Brunet, F., Dubois, K., Veizer, J., Ndondo, G.R.N., Ngoupayou, J.R.N., Boeglin, J.L., Probst, J.L., 2009. Terrestrial and fluvial carbon fluxes in a tropical watershed: Nyong basin, Cameroon. Chem. Geol. 265, 563–572.
Burkhardt, S.G., Riebesell, U., Zondervan, I., 1999. Effects of growth rate, CO_2 concentration, and cell size on the stable carbon isotope fractionation in marine phytoplankton. Geochim. Cosmochim. Acta 63, 3729–3741.
Carré, M., Sachs, J.P., Purca, S., Schauer, A.J., Braconnot, P., Falcón, R.A., Julien, M., Lavallée, D., 2014. Holocene history of ENSO variance and asymmetry in the eastern tropical Pacific. Science 345, 1045–1048.
Castañeda, I.S., Mulitza, S., Schefuß, E., Lopes dos Santos, R.A., Sinninghe Damsté, J.S., Schouten, S., 2009. Wet phases in the Sahara/Sahel region and human migration patterns in North Africa. Proc. Natl. Acad. Sci. U. S. A. 106, 20159–20163.
Cerling, T.E., Harris, J.M., MacFadden, B.J., Leakey, M.G., Quade, J., Eisenmann, V., Ehleringer, J.R., 1997. Global vegetation change through the Miocene/Pliocene boundary. Nature 389, 153–158.
Chiang, J.C.H., Friedman, A.R., 2012. Extratropical cooling, interhemispheric thermal gradients, and tropical climate change. Annu. Rev. Earth Planet. Sci. 40, 383–412.
Chikaraishi, Y., Naraoka, H., 2003. Compound-specific δD–$\delta^{13}C$ analyses of *n*-alkanes extracted from terrestrial and aquatic plants. Phytochemistry 63, 361–371.
Clement, A.C., Seager, R., Cane, M.A., 2000. Suppression of El Niño during the mid-Holocene by changes in the Earth's orbit. Paleoceanography 15, 731–737. http://dx.doi.org/10.1029/1999PA000466.
Collister, J., Reiley, G., Stern, B., Eglinton, G., Fry, B., 1994. Compound-specific $\delta^{13}C$ analyses of leaf lipids from plants with differing carbon dioxide metabolisms. Org. Geochem. 21, 619–627.
Conroy, J.L., Overpeck, J.T., Cole, J.E., Shanahan, T.M., Steinitz-Kannan, M., 2008. Holocene changes in eastern tropical Pacific climate inferred from a Galápagos lake sediment record. Quat. Sci. Rev. 27, 1166–1180.
Denniston, R.F., Wyrwoll, K.-H., Polyak, V.J., Brown, J.R., Asmerom, Y., Wanamaker Jr., A.D., LaPointe, Z., Ellerbroek, R., Barthelmes, M., Cleary, D., Cugley, J., Woods, D., Humphrey, W.F., 2013. A stalagmite record of Holocene IndonesianeAustralian summer monsoon variability from the Australian tropics. Quat. Sci. Rev. 78, 155–168.
Dykoski, C.A., Edwards, R.L., Cheng, H., Yuan, D., Cai, Y., Zhang, M., Lin, Y., Qing, J., An, Z., Revenaugh, J., 2005. A high-resolution, absolute-dated Holocene and deglacial Asian monsoon record from Dongge Cave, China. Earth Planet. Sci. Lett. 233, 71–86.
Eglinton, G., Hamilton, R.J., 1967. Leaf epicuticular waxes. Science 156 (3780), 1322.
Ehleringer, J.R., Cerling, T.E., Helliker, B.R., 1997. C_4 photosynthesis, atmospheric CO_2, and climate. Oecologia 112, 285–299.
Ehleringer, J.R., 2005. The influence of atmospheric CO_2, temperature, and water on the abundance of C3/C4 taxa. In: Ehleringer, J.R., Cerling, T.E., Dearing, M.D. (Eds.), A History of Atmospheric CO_2 and its Effect on Plants, Animals, and Ecosystems. Springer Verlag, NY, pp. 214–231.

Epstein, H.E., Lauenroth, W.K., Burke, I.C., Coffin, D.P., 1997. Productivity patterns of C3 and C4 functional types in the U.S. Great Plains. Ecology 78, 722–731.

Fleitmann, D., Burns, S.J., Mangini, A., Mudelsee, M., Kramers, J., Villa, I., Neff, U., Al-Subbarye, A.A., Buettner, A., Hippler, D., Matter, A., 2007. Holocene ITCZ and Indian monsoon dynamics recorded in stalagmites from Oman and Yemen (Socotra). Quat. Sci. Rev. 26, 170–188.

Fogel, M.L., Cifuentes, L.A., 1993. Isotope fractionation during primary production. In: Engel, M.H., Macko, S.A. (Eds.), Organic Geochemistry. Plenum Press, New York, pp. 73–98.

Gao, Y., Wang, H.J., 2012. Pan-Asian monsoon and its definition, principal modes of precipitation, and variability features. Sci. China Earth Sci. 55, 787–795.

Haug, G.H., Hughen, K.A., Sigman, D.M., Peterson, L.C., Röhl, U., 2001. Southward migration of the intertropical convergence zone through the Holocene. Science 293, 1304–1308.

Herzschuh, U., 2006. Palaeo-moisture evolution in monsoonal Central Asia during the last 50,000 years. Quat. Sci. Rev. 25, 163–178.

Huang, E., Tian, J., Steinke, S., 2011. Millennial-scale dynamics of the winter cold tongue in the southern South China Sea over the past 26 ka and the East Asian winter monsoon. Quat. Res. 75, 196–204.

Huang, R.H., Wu, Y.F., 1989. The influence of ENSO on the summer climate change in China and its mechanism. Adv. Atmos. Sci. 6, 21–32.

Indermühle, A., et al., 1999. Holocene carbon-cycle dynamics based on CO_2 trapped in ice at Taylor Dome, Antarctica. Nature 398, 121–126.

Karim, A., Veizer, J., 2000. Weathering processes in the Indus River Basin: implications from riverine carbon, sulfur, oxygen, and strontium isotopes. Chem. Geol. 170, 153–177.

Keeley, J.E., Rundel, P.W., 2003. Evolution of CAM and C_4 carbon-concentrating mechanisms. Int. J. Plant Sci. 164, S55–S77.

Kong, D.M., Zong, Y.Q., Jia, G.D., Wei, G.J., Chen, M.-T., Liu, Z.H., 2014. The development of late Holocene coastal cooling in the northern South China Sea. Quat. Int. 349, 300–307.

Koutavas, A., deMenocal, P.B., Olive, G.C., Lynch-Stieglitz, J., 2006. Mid-Holocene El Niño–Southern Oscillation (ENSO) attenuation revealed by individual foraminifera in eastern tropical Pacific sediments. Geology 34, 993–996.

Koutavas, A., Joanides, S., 2012. El Niño–Southern oscillation extrema in the Holocene and Last Glacial Maximum. Paleoceanography 27, PA4208. http://dx.doi.org/10.1029/2012PA002378.

Laws, E.A., Popp, B.N., Bidigare, R.R., Kennicutt, M.C., Macko, S.A., 1995. Dependence of phytoplankton carbon isotopic composition on growth rate and $[CO_2]_{aq}$: theoretical considerations and experimental results. Geochim. Cosmochim. Acta 59, 1131–1138.

Leduc, G., Schneider, R., Kim, J.-H., Lohmann, G., 2010. Holocene and Eemian sea surface temperature trends as revealed by alkenone and Mg/Ca paleothermometry. Quat. Sci. Rev. 29, 989–1004.

Lehmann, M.F., Bernasconi, S.M., McKenzie, J.A., Barbieri, A., Simona, M., Veronesi, M., 2004. Seasonal variation in the $\delta^{13}C$ and $\delta^{15}N$ of particulate and dissolved carbon and nitrogen in Lake Lugano: constraints on biogeochemical cycling in a eutrophic lake. Geochim. Cosmochim. Acta 49, 415–429.

Linsley, B.K., Rosenthal, Y., Oppo, D.W., 2010. Holocene evolution of the Indonesian throughflow and the western Pacific warm pool. Nat. Geosci. 3, 578–583.

Liu, J.Q., Lu, H.Y., Negendank, J., Mingram, J., Luo, X.J., 2000. Periodicity of Holocene climatic variations in the Huguangyan Maar Lake. Chin. Sci. Bull. 45, 1712–1717.

Liu, K.-K., Kao, S.-J., Chiang, K.-P., Gong, G.-C., Chang, J., Cheng, J.-S., Lan, C.-Y., 2013. Concentration dependent nitrogen isotope fractionation during ammonium uptake by phytoplankton under an algal bloom condition in the Danshuei estuary, northern Taiwan. Mar. Chem. 157, 242–252.

Liu, T.S., Ding, Z.L., 1998. Chinese loess and the paleomonsoon. Annu. Rev. Earth Planet. Sci. 26, 111–145.

Maher, B.A., 2008. Holocene variability of the East Asian summer monsoon from Chinese cave records: a re-assessment. Holocene 18, 861–866.

Maher, B.A., Tompson, R., 2012. Oxygen isotopes from Chinese caves: records not of monsoon rainfall but of circulation regime. J. Quat. Sci. 27, 615–624.

Mariotti, A., Landreau, A., Simon, B., 1988. ^{15}N biogeochemistry and natural denitrification process in groundwater: application to the chalk aquifer of northern France. Geochim. Cosmochim. Acta 52, 1869–1978.

McGregor, H.V., Gagan, M.K., 2004. Western Pacific coral $\delta^{18}O$ records of anomalous Holocene variability in the El Niño–Southern Oscillation. Geophys. Res. Lett. 31, L11204. http://dx.doi.org/10.1029/2004GL019972.

McLauchlan, K.K., Williams, J.J., Craine, J.M., Jeffers, E.S., 2013. Changes in global nitrogen cycling during the Holocene epoch. Nature 495, 352–355.

Meyers, P.A., 1997. Organic geochemical proxies of paleoceanographic, paleolimnologic, and paloclimatic processes. Org. Geochem. 27, 213–250.

Mingram, J., Schettler, G., Nowaczyk, N.R., Luo, X., Lu, H.Y., Liu, J.Q., Negendank, J.F.W., 2004. The Huguang maar Lake a high-resolution record of palaeoenvironmental and palaeoclimatic changes over the last 78,000 years from South China. Quat. Int. 122 (1), 85–107.

Moy, C.M., Seltzer, G.O., Rodbell, D.T., Anderson, D.M., 2002. Variability of El Niño/Southern Oscillation activity at millennial timescales during the Holocene epoch. Nature 420, 162–165.

Peters, K.E., Moldowan, J.M., 1993. The Biomarker Guide, Interpreting Molecular Fossils in Petroleum and Ancient Sediments. Prentice Hall, p. 363.

Porter, S.C., Zhou, W.J., 2006. Synchronism of Holocene East Asian monsoon variations and North Atlantic drift-ice tracers. Quat. Res. 65 (3), 443–449.

Polissar, P.J., Abbott, M.B., Wolfe, A.P., Vuille, M., Bezada, M., 2013. Synchronous interhemispheric Holocene climate trends in the tropical Andes. Proc. Natl. Acad. Sci. U. S. A. 110, 14551–14556.

Quay, P.D., Wilbur, D.O., Richey, J.E., Hedges, J.I., Devol, A.H., Victoria, R., 1992. Carbon cycling in the Amazon River: implications from the $\delta^{13}C$ compositions of particles and solutes. Limnol. Oceanogr. 37, 857–871.

Ran, M., Feng, Z.D., 2013. Holocene moisture variations across China and driving mechanisms: a synthesis of climatic records. Quat. Int. 313–314, 179–193.

Rau, G.H., Takahashi, T., Des Marais, D.J., Repeta, D.J., Martin, J.H., 1992. The relationship between $\delta^{13}C$ of organic matter and $[CO_{2(aq)}]$ in surface water: data from a JGOFS site in the northeast Atlantic Ocean and a model. Geochim. Cosmochim. Acta 56, 1413–1419.

Shen, J., Wu, X., Zhang, Z., Gong, W., He, T., Xu, X., Dong, H., 2013. Ti content in Huguangyan maar lake sediment as a proxy for monsoon-induced vegetation density in the Holocene. Geophys. Res. Lett. 40, 5757–5763.

Shuman, B., Henderson, A.K., Colman, S.M., Stone, J.R., Fritz, S.C., Stevens, L.R., Power, M.J., Whitlock, C., 2009. Holocene lake-level trends in the Rocky Mountains, USA. Quat. Sci. Rev. 28, 1861–1879.

Steinke, S., Mohtadi, M., Groeneveld, J., Lin, L.-C., Löwemark, L., Chen, M.-T., Rendle-Bühring, R., 2010. Reconstructing the southern South China Sea upper water column structure since the Last Glacial Maximum: implications for the East Asian winter monsoon development. Paleoceanography 25, PA2219. http://dx.doi.org/10.1029/2009PA001850.

Steinke, S., Glatz, C., Mohtadi, M., Groeneveld, J., Li, Q., Jian, Z., 2011. Past dynamics of the East Asian monsoon: no inverse behaviour between the summer and winter monsoon during the Holocene. Glob. Planet. Change 78, 170–177.

Strong, D., Flecker, R., Valdes, P.J., Wilkinson, I.P., Rees, J.G., Michaelides, K., Zong, Y.Q., Lloyd, J.M., Yu, F.L., Pancost, R.D., 2013. A new regional, mid-Holocene palaeoprecipitation signal of the Asian Summer Monsoon. Quat. Sci. Rev. 78, 65–76.

Talbot, M.R., Lærdal, T., 2000. The Late Pleistocene-Holocene palaeolimnology of Lake Victoria, East Africa, based upon elemental and isotopic analyses of sedimentary organic matter. J. Paleolimnol. 23, 141–164.

Talbot, M.R., Jensen, N.B., Lærdal, T., Filippi, M.L., 2006. Geochemical responses to a major transgression in giant African lakes. J. Paleolimnol. 35, 467–489.

Tao, S.Y., Zhang, Q.Y., 1998. Response of the Asian winter and summer Monsoon to ENSO events. Sci. Atmos. Sin. 22, 399–407 (in Chinese with English abstract).

Telmer, K., Veizer, J., 1999. Carbon fluxes, pCO_2 and substrate weathering in a large northern river basin, Canada: carbon isotope perspectives. Chem. Geol. 159, 61–86.

Uchikawa, J., Popp, B.N., Schoonmaker, J.E., Timmermann, A., Lorenz, S.J., 2010. Geochemical and climate modeling evidence for Holocene aridification in Hawaii: dynamic response to a weakening equatorial cold tongue. Quat. Sci. Rev. 29, 3057–3066.

Wachniew, P., 2006. Isotopic composition of dissolved inorganic carbon in a large polluted river: the Vistula, Poland. Chem. Geol. 233, 293–308.

Wada, E., Hattori, A., 1978. Nitrogen isotope effects in the assimilation of inorganic nitrogenous compounds by marine diatoms. Geomicrobiol. J. 1, 85–101.

Wang, L., Lu, H.Y., Liu, J.Q., Gu, Z.Y., Mingram, J., Chu, G.Q., Li, J.J., Rioual, P., Negendank, J.F.W., Han, J.T., Liu, T.S., 2008. Diatom-based inference of variations in the strength of Asian winter monsoon winds between 17,500 and 6000 calendar years BP. J. Geophys. Res. Atmos. 113, D21101. http://dx.doi.org/10.1029/2008JD010145.

Wang, L., Li, J.J., Lu, H.Y., Gu, Z.Y., Rioual, P., Hao, Q.Z., Mackay, A.W., Jiang, W.Y., Cai, B.G., Xu, B., Han, J.T., Chu, G.Q., 2012. The East Asian winter monsoon over the last 15,000 years: its links to high-latitudes and tropical climate systems and complex correlation to the summer monsoon. Quat. Sci. Rev. 32, 131–142.

Wang, L.J., Sarnthein, M., Erlenkeuser, H., Grimalt, J., Grootes, P., Heilig, S., Ivanova, E., Kienast, M., Pelejero, C., Pflaumann, U., 1999. East Asian monsoon climate during the Late Pleistocene: high-resolution sediment records from the South China Sea. Mar. Geol. 156, 245–282.

Wang, S.Y., Lu, H.Y., Liu, J.Q., Negendank, J.F.W., 2007. The early Holocene optimum inferred from a high-resolution pollen record of Huguangyan Maar Lake in southern China. Chin. Sci. Bull. 52, 2829–2836.

Wang, Y.B., Liu, X.Q., Herzschuh, U., 2010. Asynchronous evolution of the Indian and East Asian Summer Monsoon indicated by Holocene moisture patterns in monsoonal central Asia. Earth Sci. Rev. 103, 135–153.

Wang, Y.J., Cheng, H., Edwards, R.L., He, Y.Q., Kong, X.G., An, Z.S., Wu, J.Y., Kelly, M.J., Dykoski, C.A., Li, X.D., 2005. The Holocene Asian monsoon: links to solar changes and North Atlantic climate. Science 308, 854–857.

Wang, Y.M., Ren, F.M., Li, W.J., Wang, X.L., 2008. Climatic characteristics of typhoon precipitation over China. J. Trop. Meteorol. 24, 233–238 (in Chinese with English abstract).

Wang, Y.V., Larsen, T., Leduc, G., Andersen, N., Blanz, T., Schneider, R.R., 2013. What does leaf wax δD from amixed C3/C4 vegetation region tell us? Geochim. Cosmochim. Acta 111, 128–139.

Waser, N.A.D., Harrison, P.J., Nielsen, B., Calvert, S.E., Turpin, D.H., 1998. Nitrogen isotope fractionation during the uptake and assimilation of nitrate, nitrite, ammonium, and urea by a marine diatom. Limnol. Oceanogr. 43 (2), 215–224.

Wu, M.C., Chang, W.L., Leung, W.M., 2004. Impacts of El Niño–Southern Oscillation events on tropical cyclone landfalling activity in the western North Pacific. J. Clim. 17, 1419–1428.

Wu, X.D., Zhang, Z.H., Xu, X.M., Shen, J., 2012. Asian summer monsoonal variations during the Holocene revealed by Huguangyan maar lake sediment record. Palaeogeogr. Palaeoclimatol. Palaeoecol. 323–325, 13–21.
Xie, S.C., Evershed, R.P., Huang, X.Y., Zhu, Z.M., Pancost, R.D., Meyers, P.A., Gong, L.F., Hu, C.Y., Huang, J.H., Zhang, S.H., Gu, Y.S., Zhu, J.Y., 2013. Concordant monsoon-driven postglacial hydrological changes in peat and stalagmite records and their impacts on prehistoric cultures in central China. Geology 41, 827–830.
Yancheva, G., Nowaczyk, N.R., Mingram, J., Dulski, P., Schettler, G., Negendank, J.F.W., Liu, J.Q., Sigman, D.M., Peterson, L.C., Haug, G.H., 2007. Influence of the intertropical convergence zone on the East Asian monsoon. Nature 445, 74–77.
Yang, S.L., Ding, Z.L., 2008. Advance-retreat history of the East-Asian summer monsoon rainfall belt over northern China during the last two glacial-intergalcial cycles. Earth Planet. Sci. Lett. 274, 499–510.
Yang, X.P., Wang, X.L., Liu, Z.T., Li, H.W., Ren, X.Z., Zhang, D.G., Ma, Z.B., Rioual, P., Jin, X.D., Scuderi, L., 2013. Initiation and variation of the dune fields in semi-arid China – with a special reference to the Hunshandake Sandy Land, Inner Mongolia. Quat. Sci. Rev. 78, 369–380.
Yang, X.Q., Liu, Q.S., Duan, Z.Q., Su, Z.H., Wei, G.J., Jia, G.D., Ouyang, T.P., Su, Y.L., Xie, L.H., 2012. A Holocene palaeomagnetic secular variation record from Huguangyan maar Lake, southern China. Geophys. J. Int. 190, 188–200.
Zhang, C.X., Sun, X.L., Xie, S.Y., Xie, L.L., Zhan, D.L., 2008. The phytoplankton of the Huguangyan maar lake. Acta Hydrobiol. Sin. 32, 620–630 (in Chinese with an English abstract).
Zhang, J.W., Chen, F.H., Holmes, J.A., Li, H., Guo, X.Y., Wang, J.L., Li, S., Lü, Y.B., Zhao, Y., Qiang, M.R., 2011. Holocene monsoon climate documented by oxygen and carbon isotopes from lake sediments and peat bogs in China: a review and synthesis. Quat. Sci. Rev. 30, 1973–1987.
Zhao, Y., Yu, Z.C., Chen, F.H., Zhang, J.W., Yang, B., 2009a. Vegetation response to Holocene climate change in monsoon-influenced region of China. Earth Sci. Rev. 97, 242–256.
Zhao, Z.G., 1996. Impact of El Niño events on atmospheric circulations in the northern Hemisphere and precipitation in China. Sci. Atmos. Sin. 20, 422–428 (in Chinese with English Abstract).
Zhou, H.Y., Guan, H.Z., Chi, B.Q., 2007. Record of winter monsoon strength. Nature 450 (7168), E10–E11.
Zhou, H.Y., Wang, B., Guan, H.Z., Lai, Y., You, C., Wang, J.L., Yang, H., 2009b. Constraints from strontium and neodymium isotopic ratios and trace elements on the sources of the sediments in Lake Huguang Maar. Quat. Res. 72 (2), 289–300.